An Inductive and Capacitive Combined Parallel Transmission of Power and Data for Wireless Power Transfer Systems

Xiaofei Li, *Student Member, IEEE*, Chunsen Tang, *Member, IEEE*, Xin Dai, *Member, IEEE*, Pengqi Deng, and Yugang Su, *Member, IEEE*

***Abstract*—A new parallel transmission method of power and data is proposed for peer-to-peer wireless power transfer (WPT) systems. Essentially, data are modulated and transferred via high-frequency electric field generated by the parasitic capacitances of the coupling coils and the metal shield plates, while power is transferred through relatively low-frequency magnetic field generated by the coupling coils. Coupling structure and operation principle are illustrated and analyzed. Besides, the signal to noisy ratio performance is studied and optimized. With the proposed method, a 40 W prototype is built and the data transmission rate reaches 230 kbps. Experimental results have verified that the proposed method is valid and has the advantages of good flexibility and large spatial position offset redundancy. Because the method does not do any modification on the main circuit of the WPT system, it also has advantages of low cost and easy to implement.**

***Index Terms*—Data transfer, parasitic capacitances, wireless power transfer (WPT).**

I. Introduction

Wireless power transfer (WPT) technology, which is developed to contactlessly deliver power to electrical devices, has attracted worldwide attention in recent years [1]–[3]. Combined with a wireless data transfer technology, it can provide an ideal solution for the requirements of flexible, reliable, and safe power and data transmission in applications of drilling systems, electric vehicles, implanted artificial organs, etc. [1], [4], [5]. There already have some good wireless data transmission technologies such as Bluetooth, ZigBee, Wi-Fi, and radio-frequency (RF) communication, but one thing is that the complicated pairing of the transmitting and receiving sides is needed in these technologies. And what is more, the relatively high cost and long transmission delay (up to several milliseconds [6]) motivate people to keep trying to achieve fast online data communication on existing power transfer channels of WPT systems [7], [8].

It should be noted that the "WPT" system studied in this paper refers to inductive power transfer (IPT), which realizes the power transfer through inductive coupling. The parallel transmission of power and data in IPT system has been widely studied. The main methods are: 1) to transfer data at the power coupling coils by modulating data on power waveforms [1], [7], [9]; and 2) to transfer data and power in parallel by adding an auxiliary pair of data coupling coils [10]. Both of the above-mentioned ways are to transfer data via magnetic field, and the feasibility has been verified. But the following insufficiencies should be taken into consideration: for the method 1), additional harsh bandpass filters are needed, and the data transfer may affect the power transfer; for the method 2), additional coils are needed, the volume of coupling structure will be increased.

In a practical peer-to-peer IPT system (such as wireless charging system for electric vehicles, robots, or automatic-guided vehicles), usually the metal shield plates are placed on both primary and secondary sides to shield the stray magnetic field. And it has been studied that the parasitic capacitances in the coupling twisted coils cannot be ignored [11]–[13] when the operating frequency is high. Shadmand and Balog [14] propose a finite-element analysis approach to quantitatively determine the parasitic capacitances of high-frequency multiwinding transformers. Tang *et al*. [12], [13] illustrate the power transfer via the coreless printed circuit board transformers when considering the parasitic capacitances, whereas the data transmission is not mentioned. Wang and Sanders [15] propose a contactless USB capacitive power and bidirectional data transfer method, the data transfer speed reaches 100 Mb/s whereas the transferred power is relatively low as 1.25 W.

To realize the parallel transmission of power and data in WPT system, in this paper, we introduce a new method, which transfers data in a capacitive way while transferring power in an inductive way. Data are transferred via the parasitic capacitances of the coupling coils and the metal shield plates, while power is transferred through the coupling coils. Comparing the proposed method with the traditional ways, no additional coils

Manuscript received March 13, 2017; revised May 29, 2017; accepted July 4, 2017. Date of publication July 11, 2017; date of current version February 22, 2018. This work was supported in part by the research funds for the National Natural Science Foundation of China under Grants 51377183, 51477020, and 61573074, in part by the Chongqing International Science and Technology Cooperation Base Project under Grant CSTC2015GJHZ40001, and in part by the Fundamental Research Funds for the Central Universities under Grant 106112016CDJXZ178801. Recommended for publication by Associate Editor C. T. Rim. *(Corresponding author: Chunsen Tang.)*

The authors are with the School of Automation, Chongqing University, Chongqing 400044, China (e-mail: 569411680@qq.com; cstang@cqu.edu.cn; toybear@vip.sina.com; 357619947@qq.com; su7558@qq.com).

Color versions of one or more of the figures in this paper are available online at http://ieeexplore.ieee.org.

Digital Object Identifier 10.1109/TPEL.2017.2725990

are needed, and the bandpass filter is easy to design because the power is transferred by magnetic field while the data are transferred by electric field. With the proposed method, a 40 W prototype is built, and the transferred data speed reaches 230 kbps. Experimental results have shown that data transfer channel almost has no effect on power transfer, and the proposed method has the advantages of good flexibility and large spatial position offset redundancy.

II. Coupling Structure and Principle of the Power and Data Transfer

A. *Coupling Structure and Calculation of the Parasitic Capacitances*

In practical case of "peer-to-peer" WPT systems, the coupling structure is usually as shown in Fig. 1(a), which consists of a pair of coupling coils for power transfer and a pair of aluminum plates for cancelling the magnetic field outside the power transfer area by induced eddy current. Normally, there also should be a layer of magnetic core (such as ferrite core) between the coils and the shield plates to improve the mutual inductance between the coupling coils [8]. To construct the data channel via the parasitic capacitances in the coupling structure, four terminals (*a*, *b*, *c*, and *d*) are defined as shown in Fig. 1(a), where *a* and *b* are connected to the primary and secondary coils; *d* and *c* are connected to the primary and secondary metal plates, respectively. The data carrier is injected and received through the ports (*a*, *d*) and (*b*, *c*), respectively, for the forward data transfer (data are transferred from primary side to secondary side), while the data carrier is injected and received by the ports (*b*, *c*) and (*a*, *d*), respectively, for the backward data transfer (data are transferred from secondary side to primary side).

To make a clear illustration of the parasitic capacitances in the coupling structure, a simplified structure is shown in Fig. 1(b), where the aluminum plates and ferrite cores are treated as a pair of metal shield plates [16]. The circuit model of the coupling structure is shown in Fig. 1(c).

As shown in Fig. 1(b) and (c), there are six parasitic capacitances existing in the coupling structure between the coils, between the shield plates, and between the coils and plates, which are labeled as C_{e1}, C_{e2}, C_{e3}, C_{e4}, C_{e5}, and C_{e6}, respectively. The parasitic capacitances can be estimated by

$$C = \varepsilon \frac{\sigma S}{d} \tag{1}$$

where *S* is the coupling area between the coupling objects (i.e., coupling coils or the metal shield plates). *d* is the distance between the coupling objects, and ε is a comprehensive coefficient reflecting the permittivity of the dielectric mediums between the coupling objects. σ is the coefficient of the effective coupling area. For the metal shield plates, $\sigma = 1$ since there are no gaps in the metal shield plates. As for the coupling coils, the cross section of the coupling coil is shown in Fig. 2 [14]. In the enlarge part of the cross section, *r* is the radius of the conductor, while t_r is the thickness of the insulation coating. So σ can be

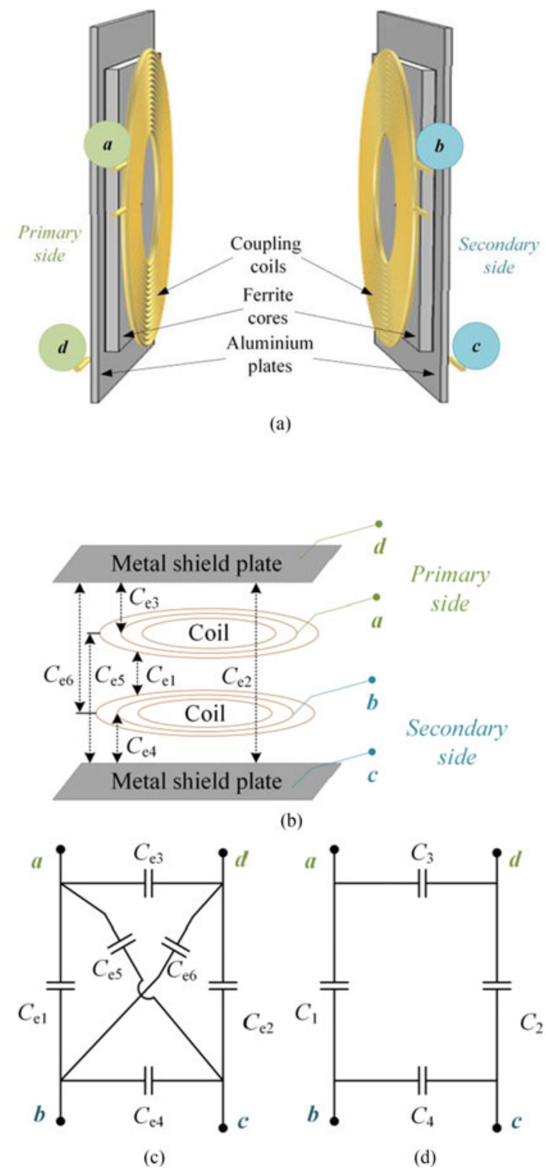

Fig. 1. Coupling structure of WPT system and its circuit model. (a) Coupling structure of a peer-to-peer WPT system; (b) simplified coupling structure; (c) circuit model of the coupling structure; and (d) simplified circuit model of the coupling structure.

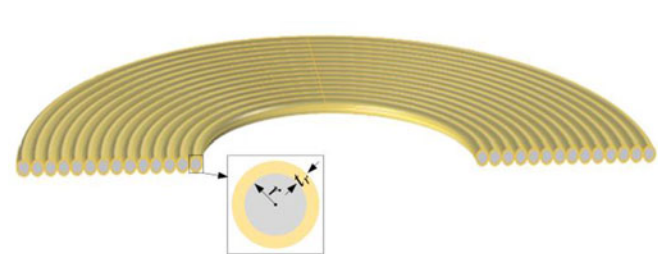

Fig. 2. Cross section of the coupling coil.

expressed as

$$\sigma = \frac{r}{r + t_r}. \tag{2}$$

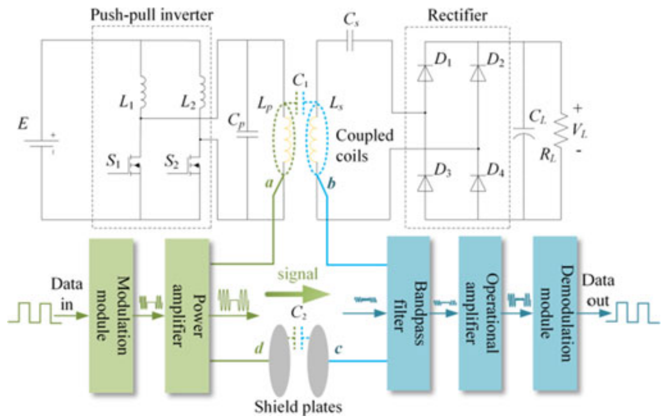

Fig. 3. System topology for power and data transmission.

The circuit model shown in Fig. 1(c) can be simplified as shown in Fig. 1(d) according to [2]. The simplified circuit shows that C_1 and C_2 are the dominant capacitances providing a path for data transmission. C_3 and C_4 are shunt capacitances at transmitter and receiver sides which may weaken the received data carrier slightly. To simplify the analysis, only the two dominant capacitances C_1 and C_2 will be considered in the subsequent analysis.

B. Principle of the Power and Data Transfer

Different *LC* branches (serial and parallel) in primary and secondary sides comprise four basic structures of WPT system: SS, SP, PS, and PP. The proposed data transfer method is applicable to all these four structures. In this paper, the primary parallel and secondary series compensation (PS) topology is employed as an example to illustrate the simultaneous wireless power and data transfer. The system topology is shown in Fig. 3, where the colorful part represents the forward data transmission channel. E is the input dc voltage source. (L_1, L_2) and (S_1, S_2) constitute a push–pull inverter [17], [18]. L_p and C_p constitute the primary parallel resonant circuit, while L_s and C_s constitute the secondary series resonant circuit. D_1–D_4 constitute the rectifier. C_L is the output filter capacitance. R_L is the load resistance. V_L is the output voltage. The parasitic capacitance C_1 is treated as a lumped capacitance and placed on the top of the coils according to [13].

As can be seen from Fig. 3, the transmitter side circuit for data transfer consists of a modulation module and a power amplifier, while the receiver (secondary) side consists of a bandpass filter, an operational amplifier, and a demodulation module. amplitude shift keying (ASK) modulation method is used to generate the data carrier. It adopts "0" and a specific frequency signal to discriminate and transmit binary data "1" and "0," respectively. The generation of the carrier can be expressed as

$$c(t) = \begin{cases} A\cos(2\pi f_d t), & ''0'' \\ 0, & ''1'' \end{cases} \tag{3}$$

where f_d and A are the operating frequency and the amplitude of the data carrier, respectively. When the transferred data bit is "1," there is no data carrier in the data channel.

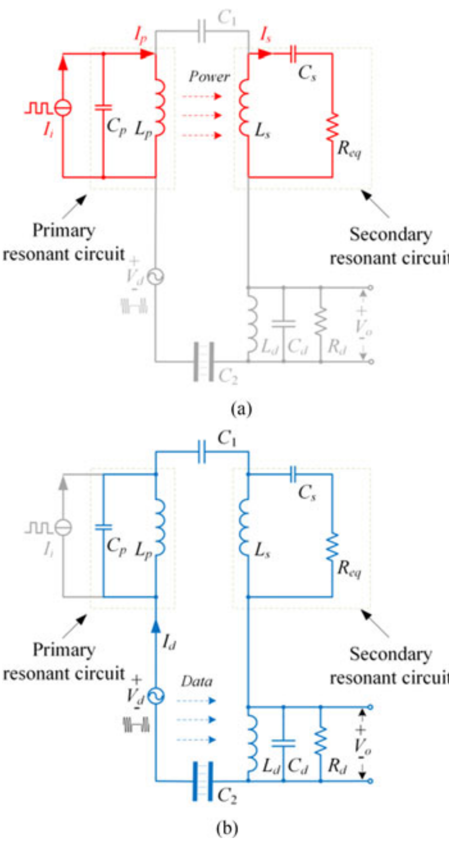

Fig. 4. Illustration of the transfer channels for power and data. (a) Power transfer channel; and (b) data transfer channel.

The simplified power transfer channel and data transfer channel are shown in Fig. 4. The input power source is represented by a square current source I_i. R_{eq} is the equivalent input resistance of the rectifier, which satisfies $R_{\mathrm{eq}}= \frac{8}{\pi^2}R_L$. V_d is the injected data carrier (the output of the power amplifier), while V_o is the received data carrier. L_d and C_d comprise an *LC* tuning circuit to maximize the output carrier V_o, satisfying $\omega_d= \frac{1}{\sqrt{L_d C_d}}$, ω_d is the angular frequency of the data carrier. R_d is the input resistance of the bandpass filter.

The power transfer channel is shown in Fig. 4(a) marked in red while the data transfer channel is shown in Fig. 4(b) marked in blue. It can be seen that the shared channel of the power and data transfer is the primary and the secondary resonant circuits. And the signal to noisy ratio (SNR) is mainly affected by the shared channel.

The following assumptions are made to simplify the analysis:

1) The data carrier frequency f_d is selected at least an order of magnitude higher than the power carrier frequency f_p [7], [10], that because: a) the power transfer efficiency would not be significantly affected by data transfer channel; and b) the bandpass filter is easy to design to suppress the interference from power transfer to data transfer. The carrier frequency ratio is defined as

$$\alpha = \frac{\omega_d}{\omega_p} = \frac{f_d}{f_p}. \tag{4}$$

2) The resonant frequencies of the primary and secondary sides are identical

$$\omega_p = 2\pi f_p = \frac{1}{\sqrt{L_p C_p}} = \frac{1}{\sqrt{L_s C_s}}. \tag{5}$$

III. System Performance Analysis

A. Influence on Power Transfer Due to Extra Data Transfer Channel

When considering the influence on power transfer due to the adding of the extra data transfer channel, two issues need to be considered. One is the power transfer losses due to the adding of data transfer circuits; another is the interference of data carrier transfer on power transfer. Since the power link resonates at a much lower frequency than the data carrier frequency and C_1, C_2 are very small, the impedances of these two capacitances should be very high at the power transfer frequency. These high impedances significantly limit the current in the data transfer channel. Therefore, this current will be much smaller than the currents I_p and I_s in the power transfer circuits, so the power transfer efficiency loss due to the data transfer channel can be neglected. Besides, the data carrier is negligible compared with the power carrier capacity. So the interference of data transfer on power transfer can also be ignored. The attenuation of the power transfer due to the adding of data transfer channel will be further studied in the experiment.

B. Interference of Power Transfer on Data Transfer

As mentioned before, the SNR is affected mainly from the shared channel of power transfer and data transfer shown in Fig. 4. There are two issues that should be considered for data transfer. The first is the interference of power transfer on data transfer; the second is the output data carrier capacity. These two effects could significantly influence the SNR performance. Therefore, for a well-designed data transfer channel, these two issues should be optimized. The interference of power transfer on data transfer should be minimized while the output data carrier capacity should be maximized. And these will be presented in this and the following sections.

As for the interference of power transfer on data transfer, the interference is produced due to the voltage difference between the primary resonant circuit and the secondary resonant circuit. The power transfer circuit without data carrier is shown in Fig. 5(a). M is the mutual inductance between L_p and L_s. By analyzing the power transfer operation in steady state and ignoring the data carrier transfer, the interference of power transfer on data transfer can be derived. As mentioned before, when analyzing the power transfer properties, C_1 and C_2 can be ignored, because their impedances are pretty high at the powe r frequency f_p.

The reflected impedance Z_r to the primary side is indicated by

$$Z_r = \frac{\omega^2 M^2}{Z_s} \tag{6}$$

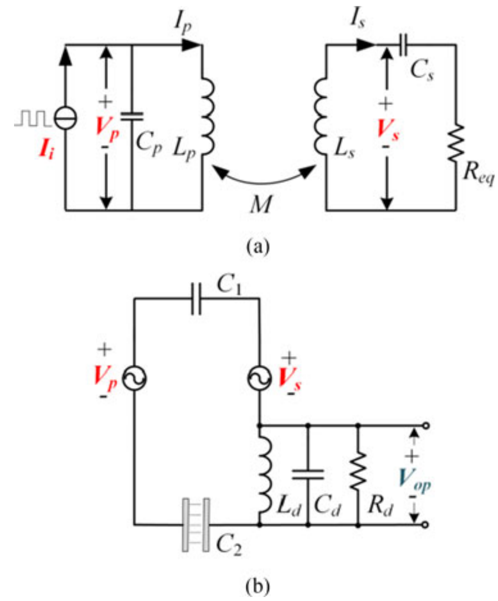

Fig. 5. Power transfer channel without data carrier. (a) Power transfer channel; and (b) interference of power transfer on data transfer.

where Z_s is the secondary loop impedance, given by $Z_s = j\omega L_s + 1/j\omega C_s + R_{\rm eq}$.

The primary inductance current I_p can be derived as

$$I_p = \frac{1}{j\omega C_p Z_{pp}} I_i \tag{7}$$

where Z_{pp} is the impedance given by $Z_{pp} = j\omega L_p + 1/j\omega C_p + Z_r$.

The secondary side current can be derived as

$$I_s = \frac{j\omega M I_p}{Z_s}. \tag{8}$$

The primary resonant circuit voltage V_p can be expressed as

$$V_p = j\omega L_p I_p - j\omega M I_s. \tag{9}$$

The secondary resonant circuit voltage V_s can be expressed as

$$V_s = j\omega M I_p - j\omega L_s I_s. \tag{10}$$

The equivalent circuit to show the interference of power transfer on data transfer is shown in Fig. 5(b), where V_p and V_s are represented by two voltage sources. The voltage difference ΔV_{ps} between V_p and V_s can be derived as

$$\Delta V_{ps} = V_p - V_s = I_i \frac{\omega\left(j\omega M\left(L_s - M\right) + Z_s\left(L_p - M\right)\right)}{\omega^3 C_p M^2 + jZ_s\left(\omega^2 L_p C_p - 1\right)}. \tag{11}$$

So the transfer function from the power input I_i to the voltage difference ΔV_{ps} is

$$G_{pp} = \frac{\Delta V_{ps}}{I_i} = \frac{\omega\left(j\omega M\left(L_s - M\right) + Z_s\left(L_p - M\right)\right)}{\omega^3 C_p M^2 + jZ_s\left(\omega^2 L_p C_p - 1\right)}. \tag{12}$$

The output interference voltage V_{op} of power transfer on data transfer can be derived as

$$V_{\mathrm{op}} = \frac{1/\left(j\omega C_d + 1/j\omega L_d + 1/R_d\right)}{1/\left(j\omega C_d + 1/j\omega L_d + 1/R_d\right) + 1/j\omega C_1 + 1/j\omega C_2} \Delta V_{ps}. \tag{13}$$

So the transfer function from the power input I_i to the data output V_{op} is

$$G_{pd} = \frac{V_{\mathrm{op}}}{I_i} = \frac{1/\left(j\omega C_d + 1/j\omega L_d + 1/R_d\right)}{1/\left(j\omega C_d + 1/j\omega L_d + 1/R_d\right) + 1/j\omega C_1 + 1/j\omega C_2} G_{pp}. \tag{14}$$

If the parameters L_p, C_p, L_s, and C_s satisfy the assumption shown in (5), the voltage difference ΔV_{ps} can be simplified as

$$\Delta V_{ps} = I_i L_p \left(j\omega_p \left(\frac{L_s}{M} - 1 \right) + R_{\mathrm{eq}} \left(\frac{L_p - M}{M^2} \right) \right). \tag{15}$$

Equation (15) shows that the voltage difference ΔV_{ps} is related to the parameters I_i, L_p, L_s, ω_p, $R_{\mathrm{eq}}\,(R_L)$, and *M*. So in order to reduce ΔV_{ps}, we can decrease I_i, L_p, L_s, ω_p, R_L. As for *M*, due to the loose coupling characteristic of IPT system, L_p is normally larger than *M*. So ΔV_{ps} can be reduced by increasing the mutual inductance *M*. The reduction of ΔV_{ps} can also reduce the interference of power transfer on data transfer according to (13) and the SNR will become larger consequently.

C. Data Transfer Channel Analysis

In the above-mentioned section, we have known that the reduction of power transfer interference on data transfer can be achieved by decreasing the voltage difference ΔV_{ps}. In this section, we will go on to study the increment of data carrier transfer capacity. When only data transfer in the system is considered, the circuit is shown in Fig. 6(a), where the mutual inductance couplings on primary side coil and secondary side coil are represented by two controlled voltage sources $-j\omega M I_s$ and $j\omega M I_p$, respectively.

According to Kirchhoff's voltage law and Kirchhoff's current law, the following equations can be derived:

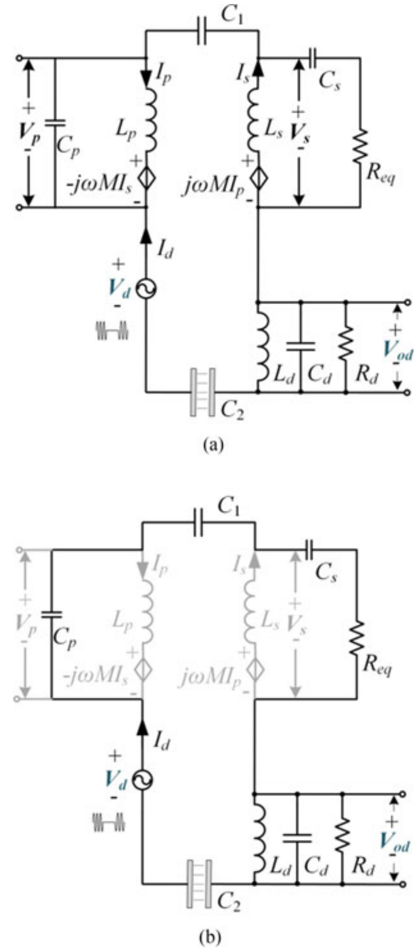

Fig. 6. Data transfer channel without power transfer. (a) Detailed data transfer channel; and (b) simplified data transfer channel.

$$\begin{cases} V_p = j\omega L_p I_p - j\omega M I_s \\ V_s = j\omega M I_p - j\omega L_s I_s \\ I_d = -I_p - \dfrac{V_p}{(1/j\omega C_p)} \\ I_d = -I_s + \frac{V_s}{(1/j\omega C_s) + R_{eq}} \\ Z_{pd} = -\frac{V_p}{I_d} \\ Z_{sd} = \frac{V_s}{I_d} \\ V_d = V_{od} + I_d\left(1/j\omega C_1 + 1/j\omega C_2\right) - V_p + V_s \\ V_{od} = I_d\left(1/\left(j\omega C_d + 1/j\omega L_d + 1/R_d\right)\right) \end{cases} \tag{16}$$

where I_d is the data channel current. Z_{pd} and Z_{sd} are the impedance of the primary and secondary resonant circuits, respectively. Z_{pd} and Z_{sd} can be solved as (17) and (18) shown at bottom of this page.

$$Z_{pd} = \frac{-j\omega\left(jC_s\omega^2\left(L_pL_s - M^2\right) + \left(j - C_sR_{eq}\omega\right)\left(L_p - M\right)\right)}{C_sR_{eq}\omega\left(C_pM\omega^2 - 1\right) + j\left(1 + L_sC_s\omega^2 - C_pM\omega^2\right)} \tag{17}$$

$$Z_{sd} = \frac{-j\omega\left(\left(C_pC_sR_{eq}\omega^2 - jC_p\omega^2\right)\left(L_pL_s - M^2\right) + \left(j - C_sR_{eq}\omega\right)\left(L_s - M\right)\right)}{C_pL_p\omega^2\left(C_sR_{eq}\omega - j\right) + j\left(1 + C_sM\omega^2\right) - C_sR_{eq}\omega} \tag{18}$$

The transfer function from the input data carrier V_d to the output data carrier V_{od} can be expressed as

$$G_{dd} = \frac{V_{od}}{V_d} = \frac{1/\left(j\omega C_d + 1/j\omega L_d + 1/R_d\right)}{\left(1/\left(j\omega C_d + 1/j\omega L_d + 1/R_d\right)\right) + 1/j\omega C_1 + 1j\omega C_2 + Z_{pd} + Z_{sd}}. \quad (19)$$

As the data carrier frequency is much larger than the power transfer frequency, the impedances of L_p and L_s should be very high at data carrier frequency, whereas the impedances of C_p and C_s should be very low at data carrier frequency. So the data transfer circuit can be simplified as shown in Fig. 6(b). As C_1 and C_2 are much lower than C_p and C_s, the impedances of C_1 and C_2 should be much larger than C_p and C_s at data carrier frequency. So the reduction of data transfer at the resonant circuits is very small. The output carrier V_{od} can be expressed as follows according to Fig. 6(b):

$$V_{od} = V_d \frac{1/\left(j\omega_d C_d + 1/j\omega_d L_d + 1/R_d\right)}{1/\left(j\omega_d C_d + 1/j\omega_d L_d + 1/R_d\right) + 1/j\omega_d C_1 + 1/j\omega_d C_2 + Z_d} \quad (20)$$

where $Z_d = 1/j\omega_d C_p + 1/j\omega_d C_s + R_{\text{eq}}$ is the simplified resonant circuits impedance at data carrier frequency.

As can be seen from (20), the output carrier is maximum when L_d and C_d resonate at data carrier frequency, satisfying $\omega_d = \frac{1}{\sqrt{L_d C_d}}$. And the maximum output carrier is

$$V_{od} = V_d \frac{R_d}{R_d + 1/j\omega_d C_1 + 1/j\omega_d C_2 + Z_d}. \quad (21)$$

Equation (21) indicates that the amplitude of the maximum output carrier can be designed to be big enough by choosing a reasonable resonant frequency ω_d.

D. Design Consideration for Demodulation

As mentioned before, the interference of power transfer on data transfer and the data carrier transfer capacity will affect the SNR performance. The SNR has to be sufficiently large, so that the received data carrier can be demodulated when the amplitude of data transfer capacity V_{od} [shown in Fig. 6(b)] is larger than the interference V_{op} [shown in Fig. 5(b)] [1]. To increase the SNR, we can either reduce the interference or increase the data transfer capacity.

To reduce the interference V_{op}, two approaches can be applied. One is to reasonably set the parameters [by decreasing L_p, L_s, ω_p, R_L and increasing the mutual inductance *M* according to (15)]. Another one is to use a filter to decrease the interference. A ceramic filter is used as the bandpass filter in this paper [19]. The filter can easily reduce the interference since the center frequency is far higher than the interference power frequency.

Similarly, to increase the output data carrier capacity V_{od}, there are also two approaches. One is to set the system parameters (by increasing data carrier frequency ω_d and set L_d and C_d resonate at the data carrier frequency). Another one is to use an operational amplifier at the output of the bandpass filter. The amplifier is used to amplify the data carrier amplitude to reach the reference voltage.

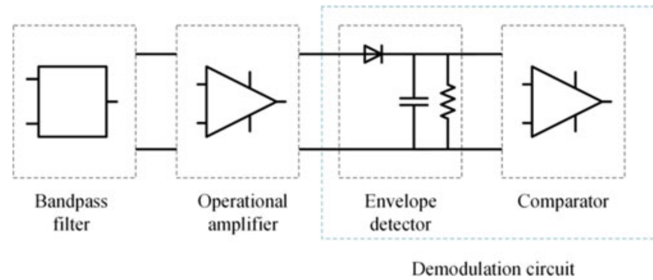

Fig. 7. Received data processing schematic circuit.

Consequently, the entire received data processing circuit can be designed as shown in Fig. 7. The previous mentioned bandpass filter and the operational amplifier are all considered in the circuit. The demodulation circuit shown in Fig. 7 consists of an envelope detector and a comparator. The envelope detector is used to get the envelope of the carrier. And the comparator is used to get the decoded data. A hysteresis comparator is utilized in this paper since it can decrease the demodulation error.

IV. Experiment Analysis of the System

A. Coupling Structure Specifications and Experiment Parameters

To verify the proposed method, an experiment prototype is built according to Fig. 3. Particularly, bidirectional data transfer channel is designed in the experiment prototype. The primary side and the secondary side of the coupling structure are designed to be the same as shown in Fig. 8(a), while the whole coupling structure is shown in Fig. 8(b). As can be seen from Fig. 8(a), the aluminum plate length is 10 cm while the ferrite core length is 8 cm. The coil inner radius is 1 cm while the coil outer radius is 4.5 cm. Fig. 8(b) shows that the coils separation distance is 2 cm. The thicknesses of the aluminum plate and the ferrite core are 1.5 and 5 mm, respectively. The detailed parameters of the system are specified in Table I, where the Litz wire diameter is 1.2 mm and the coil's number of turns is 21. The power resonant frequency is 40 kHz, while the data carrier frequency is 10 MHz. Q_p and Q_s are the quality factor of primary and secondary coils. The mutual inductance between L_p and L_s is 12.9 μH when the coils separation distance is 2 cm.

B. Normalization of the Coupling Coefficient and the Parasitic Capacitances When the Lateral Drift or the Vertical Height Varies

As mentioned before, the capacitive coupling has the advantage of large spatial position offset redundancy. The measured normalization coupling coefficient k/k_0 and parasitic capacitances C_1/C_{10} and C_2/C_{20} are shown in Fig. 9, where the reference coupling coefficient k_0 and the parasitic capacitances C_{10} and C_{20} are measured when the vertical height between the primary side and the secondary side of the coupling

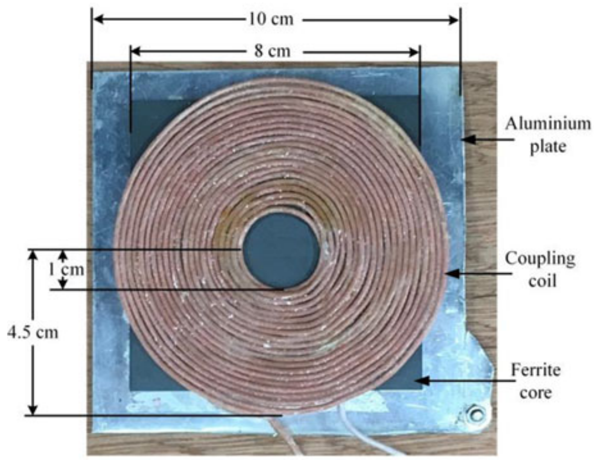

(a)

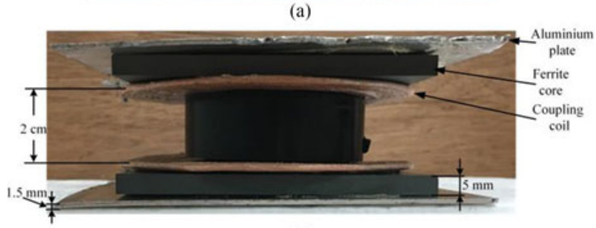

(b)

Fig. 8. Primary side and the secondary side of the coupling structure and the whole coupling structure. (a) Primary side and the secondary side of the coupling structure; and (b) whole coupling structure.

TABLE I
PARAMETERS OF THE EXPERIMENT SYSTEM

Parameter	Value	Parameter	Value
Litz wire diameter	1.2 mm	Number of turns	21
Q_p	82.7	Q_s	83.4
L_p	50 μH	L_s	50 μH
C_p	316 nF	C_s	315 nF
M	12.9 μH	E	20 V
L_1, L_2	150 μH	R_L	10 Ω
f_p	40 kHz	f_d	10 MHz

structure is 2 cm with no lateral drift ($k_0 = 0.258$, $C_{10} = 8.2\,\text{pF}$, $C_{20} = 9.1\,\text{pF}$).

Fig. 9(a) shows the normalization values with respect to the lateral drift. The lateral drift ratio (*ldr*) is defined as the drift distance divided by the coil diameter. The value varies from 0% to 30%. Fig. 9(b) shows the normalization values with respect to the vertical height. The vertical height (*vh*) varies from 2 to 5 cm. As can be seen from Fig. 9(a) and (b), the parasitic capacitances C_1 and C_2 decrease more slowly than the mutual inductance *k* when the lateral drift ratio is larger or the vertical height is larger. This indicates that the spatial position offset redundancy of the capacitive coupling is larger than that of the inductive coupling.

C. Bode Plot of Power to Data Transfer Interference and Data Transfer Capacity

The Bode plots of the interference transfer function (G_{pd}) from I_i to V_{op} and the data transfer capacity function (G_{dd})

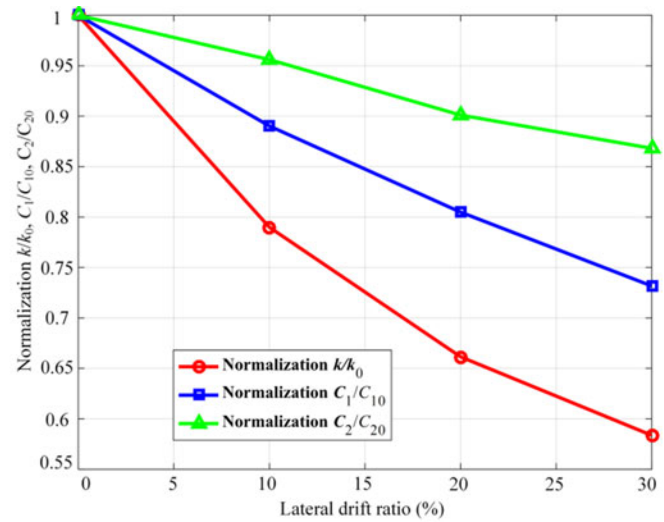

(a)

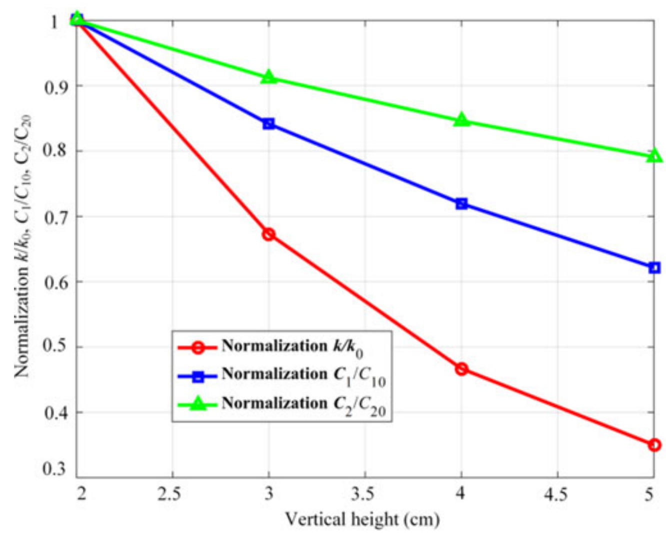

(b)

Fig. 9. Normalization of k/k_0, C_1/C_{10}, and C_2/C_{20} with respect to lateral drift and vertical height. (a) Normalization values with respect to lateral drift; and (b) normalization values with respect to vertical height.

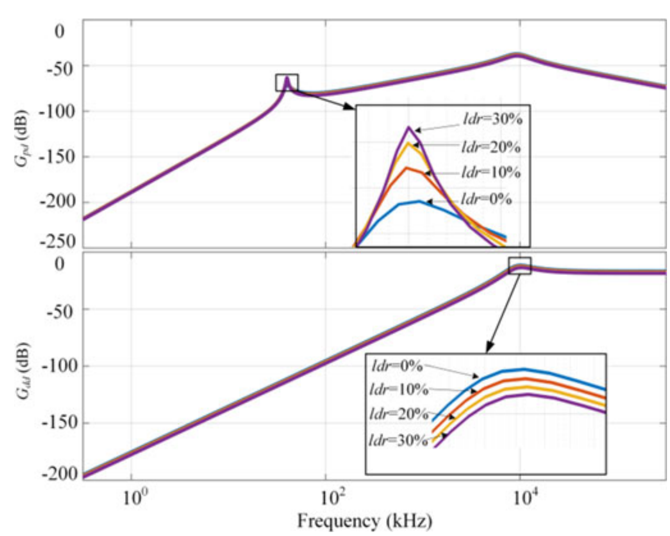

Fig. 10. Bode plots of G_{pd} and G_{dd} when the lateral drift ratio varies.

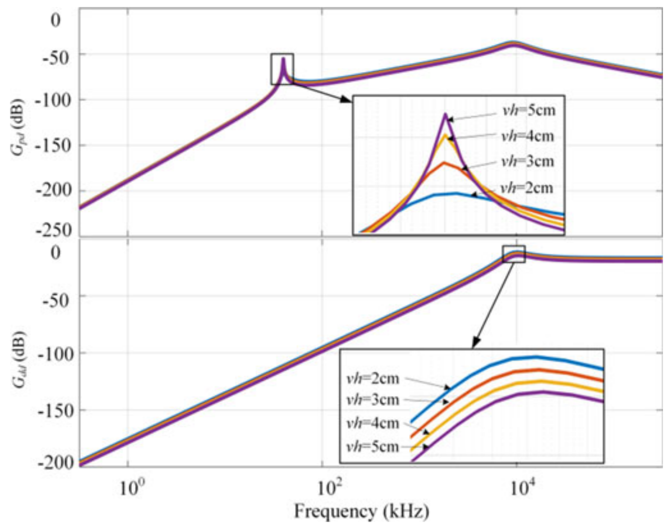

Fig. 11. Bode plots of G_{pd} and G_{dd} when the vertical height varies.

from V_d to V_{od} are shown in Fig. 10 with the lateral drift ratio (*ldr*) varying from 0% to 30%.

As can be seen from the enlarged part of Fig. 10. The interference of power transfer on data transfer at power transfer frequency (40 kHz) is larger when the lateral drift ratio is larger. The data transfer capacity at data carrier frequency (10 MHz) is smaller when the lateral drift ratio is larger. This indicates that the SNR is smaller when the lateral drift ratio is larger.

The Bode plots of the interference transfer function (G_{pd}) from I_i to V_{op} and the data transfer capacity function (G_{dd}) from V_d to V_{od} are shown in Fig. 11 when the vertical height (*vh*) varies from 2 to 5 cm.

As can be seen from the enlarged part of Fig. 11, the interference of power transfer on data transfer at power transfer frequency (40 kHz) is larger when the vertical height is larger. The data transfer capacity at data carrier frequency (10 MHz) is smaller when the vertical height is larger. This indicates that the SNR is smaller when the vertical height is larger.

D. Experiment Tests

1) Experimental Prototype and Detailed Data Transfer Circuit: To testify the effectiveness of the proposed method, experiments have been done for bidirectional data transfer. The experiment prototype photo is shown in Fig. 12, where the mentioned *a*, *b*, *c*, *d* in Fig. 1 is enclosed by a rectangle. For the primary power transfer circuit, MOSFET IRF3610 is used as the switch device of the push–pull inverter. For the secondary power transfer circuit, Schottky diode SS36 is used to construct the rectifier.

The detailed data transfer circuit is shown in Fig. 13, where the ASK modulation is produced by a CD4051 chip. The power amplifier is constructed to be a class-AB amplifier by using 2N5551 and 2N5401. A LT1816 chip is used as the operational amplifier. An LM311 chip is used as the comparator.

2) Forward Data Transfer Results When Data and Power Transfer is Normal or Standby: The typical waveforms for: 1) power transfer and data transfer are normal; 2) power transfer is normal, data transfer is standby; and 3) data transfer is normal, power transfer is standby are shown in Fig. 14(a), (b), and (c) respectively, where channel 1 is the output voltage V_L of load R_L, channel 2 is the input voltage of the bandpass filter (the output voltage V_o of R_d shown in Fig. 4), channel 3 is the output voltage of the operational amplifier, and channel 4 is the output demodulation data. It should be noted that power transfer is standby means that the input voltage E shown in Fig. 3 is power OFF. Data transfer is standby means that the transferred data is always "1," so there is no data carrier in the data transfer channel according to (3). Channel 1 waveforms shown in Fig. 14(a) and (b) indicate the output power is around 40 W. Channel 4 waveforms shown in Fig. 14(a) and (c) indicate the data transfer rate is 230 kbps (the data transfer rate is twice that of the square wave frequency).

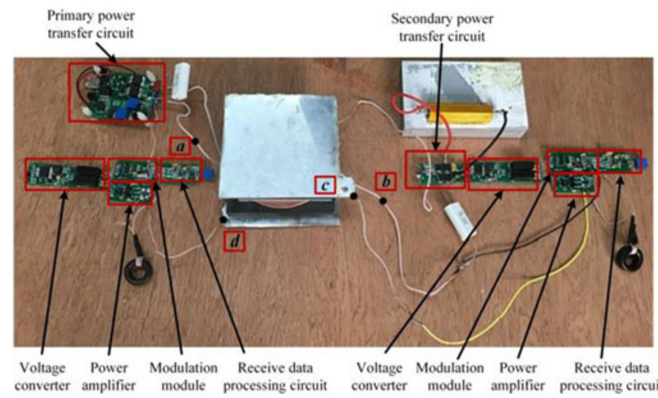

Fig. 12. Experiment prototype photo.

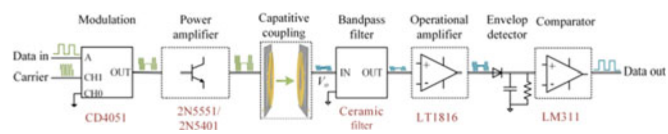

Fig. 13. Detailed data transfer circuit.

As can be seen from Fig. 14(a) and (b), the output voltage V_L is almost unchanged when data transfer is standby or normal, this is to say the interference of data transfer on power transfer is so small that it can be ignored. Channel 2 waveforms shown in Fig. 14(a) and (c) indicate that the data transfer capacity is much higher than the interference, and the SNR when the power transfer is standby is larger than that when the power transfer is normal.

3) Forward Data Transfer Experimental Results When the Lateral or Vertical Drift Varies: Fig. 14(a) shows the parallel transmission of power and data when the vertical height is 2 cm with no lateral drift. Now, we test the data transfer performance when the lateral drift ratio and vertical height vary. The results are shown in Fig. 15(a) and (b), respectively. Fig. 15(a) indicates the parallel transmission of power and data when the lateral drift ratio is 30%. Fig. 15(b) indicates the parallel transmission of power and data when the vertical height is 5 cm.

As can be seen from channel 4 waveforms shown in Fig. 15(a) and (b), even when the lateral drift ratio is 30% or the vertical height is 5 cm, the data transfer is still stable whereas the

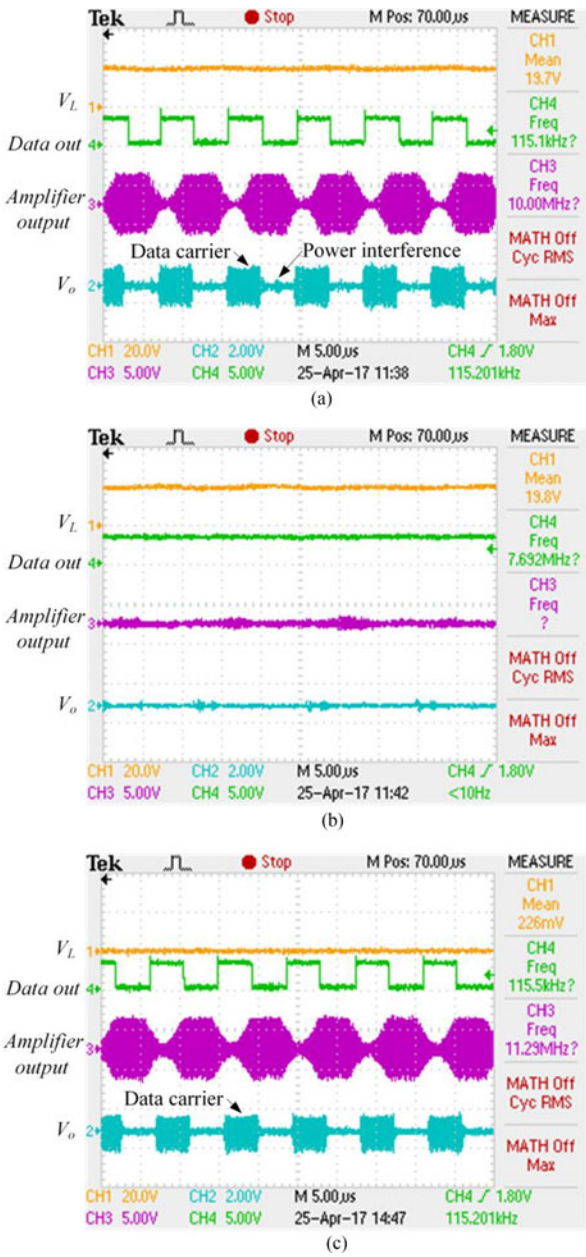

Fig. 14. Typical waveforms of system in different power and data transfer working modes. (a) Power transfer and data transfer are normal; (b) power transfer is normal, data transfer is standby; and (c) data transfer is normal, power transfer is standby.

power transfer decreases significantly compared with Fig. 14(a). Channel 1 waveform shown in Fig. 15(a) indicates the output power is 20.4 W, when the lateral drift ratio is 30%. Channel 1 waveform shown in Fig. 15(b) indicates the output power is 13.5 W, when the vertical height is 5 cm. It can also be seen that the data transfer capacity shown in channel 2 decreases greatly; the SNR is relatively small compared with Fig. 14(a). This verifies the Bode plot analysis shown in Figs. 10 and 11, i.e., the modeling of the transfer function in Section III is right.

By comparing Fig. 15(a) with 14(a), it can be seen that with the same lateral drift, V_L decreases about 25%, while V_o decreases about 12.5%. Similarly, it can be seen from Figs. 15(b) and 14(a) that with the same vertical drift, V_L decreases about 40%, while V_o decreases about 25%. Therefore, it further verifies that the performance of capacitive coupling decreases more slowly than that of inductive coupling. So we can say that the data transfer utilizing electric field has the advantage of large spatial position offset redundancy.

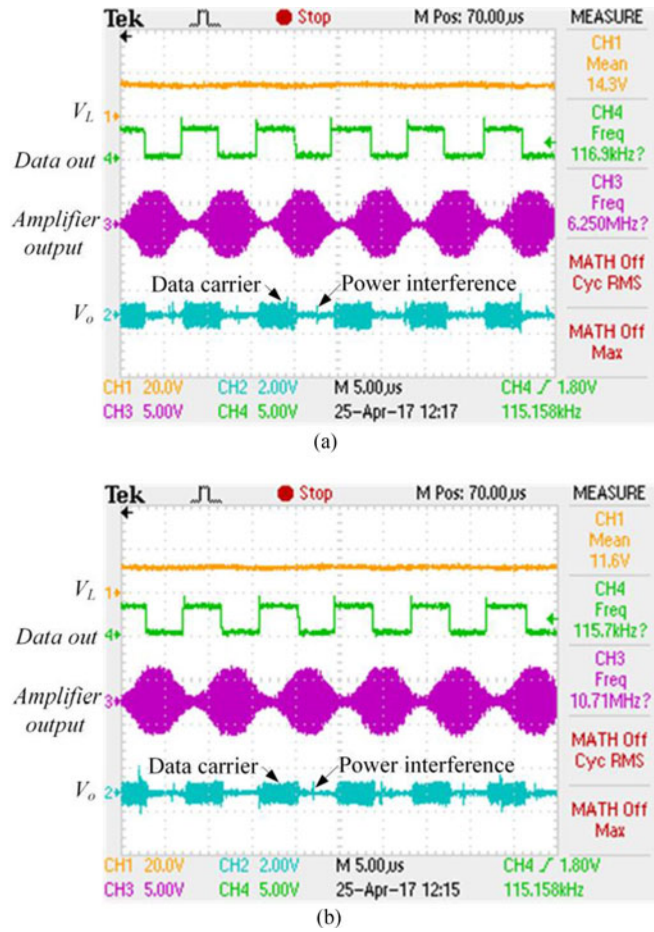

Fig. 15. Parallel transmission of power and data when the lateral drift ratio and vertical height varies. (a) Lateral drift ratio is 30%; and (b) vertical height is 5 cm.

4) Forward Data Transfer Performance Analysis: The output power and transfer efficiency of the system when the lateral drift ratio or the vertical height varies are shown in Table II, where $\mathrm{eff}_{\_\mathrm{data}}$ and P_{L_data} indicate the system efficiency and the system output power when data transfer is normal, while $\mathrm{eff}_{\_\mathrm{nodata}}$ and P_{L_nodata} correspond to that data transfer is standby (the transferred data are always in high state, i.e., there is no data carrier in data channel), $\mathrm{eff}_{\_\mathrm{plate}}$ and P_{L_plate} correspond to that the data transfer channel circuit is power OFF and the aluminum plate is not removed from the system, and $\mathrm{eff}_{\_\mathrm{noplate}}$ and P_{L_noplate} correspond to that the data transfer channel circuit is power OFF and the aluminum plate is removed from the system. By comparing P_{L_data}, P_{L_nodata}, and P_{L_plate}, we can derive that power transfer is hardly affected by data transfer (less than 1 W). As for the system efficiency, the following relationship exists: $\mathrm{eff}_{\_\mathrm{data}} < \mathrm{eff}_{\_\mathrm{nodata}} < \mathrm{eff}_{\_\mathrm{plate}} < \mathrm{eff}_{\_\mathrm{noplate}}$. $\mathrm{eff}_{\_\mathrm{data}} <$

TABLE II
EXPERIMENT RESULTS OF THE OUTPUT POWER AND EFFICIENCY WHEN THE LATERAL OR VERTICAL DRIFT VARIES

vh (cm)	*ldr* (%)	eff$_{\text{_data}}$ (%)	$P_{L\text{\_data}}$ (W)	eff$_{\text{_nodata}}$ (%)	$P_{L\text{\_nodata}}$ (W)	eff$_{\text{_plate}}$ (%)	$P_{L\text{\_plate}}$ (W)	eff$_{\text{_noplate}}$ (%)	$P_{L\text{\_noplate}}$ (W)
2	0	79.6	38.8	80.2	39.2	84.6	39.6	84.8	41.2
2	10	78.2	32.8	78.7	32.8	84.3	33.1	84.6	35.0
2	20	75.7	25.6	76.2	25.6	83.6	25.6	83.9	26.9
2	30	72.3	20.4	73.1	20.7	82.3	20.7	82.7	22.5
3	0	77.5	31.7	78.1	32.0	84.1	32.0	84.3	33.5
4	0	74.1	22.8	74.8	22.8	83.1	23.1	83.5	25.0
5	0	64.0	13.5	65.1	13.7	76.6	13.9	77.2	15.1

TABLE III
POWER INTERFERENCE AND BER RESULTS WHEN THE LATERAL DRIFT RATIO OR VERTICAL HEIGHT VARIES

vh (cm)	*ldr* (%)	Data rate (kbps)	BER (%)	$V_{\text{op-peak}}$ (V)
2	0	230	0	0.62
2	10	230	0	0.71
2	20	230	0	0.80
2	30	230	0	0.91
3	0	230	0	0.77
4	0	230	0	0.89
5	0	230	0	1.01

eff$_{\text{_nodata}}$ is due to the power consumption of the data transfer. eff$_{\text{_nodata}} <$ eff$_{\text{_plate}}$ is due to the standby power consumption of the data channel. eff$_{\text{_plate}} <$ eff$_{\text{_noplate}}$ is due to the eddy current power loss in the aluminum plate. All the output powers and the efficiencies decrease gradually with the increase of the lateral or vertical displacements.

The power transfer interference on data transfer and the bit error ratio (BER) of data transfer when the lateral drift or the vertical height varies are shown in Table III, where $V_{\text{op-peak}}$ indicates the peak value of the power transfer interference on data transfer shown in Fig. 5(b). As can be seen from Table III, the BER of data transfer is 0% when the lateral drift ratio varies from 0% to 30% or the vertical height varies from 2 to 5 cm. As for the power transfer interference on data transfer, it increases with the lateral drift ratio or the vertical height.

The SNR performance when the lateral drift or the vertical height varies is shown in Fig. 16, the results show that SNR decreases with the lateral drift ratio or the vertical height. This is consistent with the Bode plot analyses shown in Figs. 10 and 11.

5) Backward Data Transfer Experimental Results: To test the backward data transfer performance, the measured results of parallel power transfer and backward data transfer are shown in Fig. 17. It can be seen that the backward data transfer is successful. It also has been found that the performance of backward data transfer is almost the same as forward data transfer.

V. DISCUSSION

A. Superior of the Proposed Method

Table IV shows the comparison results between the proposed parallel transmission of power and data method and the inductive way studied in [1], [7], [9], and [10]. Since the data is transferred via the parasitic capacitances, no additional coils are needed, the volume of coupling structure is relatively small. Meanwhile, it can be seen from Figs. 7, 12, and 13 that the data receiving circuit is easy to design. Furthermore, the proposed data transfer method in a capacitive way also has the advantage of large spatial position offset redundancy as discussed above.

B. Data Transfer Delay of the Proposed Method

The data transfer delay of the proposed method can be studied from the waveforms shown in Fig. 18, where channel 1 indicates the input data, channel 2 indicates the received data carrier V_o (input voltage of the bandpass filter), channel 3 indicates the output voltage of the operational amplifier, and channel 4 indicates the output data. As can be seen from channel 1 and channel 2 shown in Fig. 18, there is negligible transfer delay between the input data and V_o. Transfer delay between V_o and the output voltage of operational amplifier is t_{da}. Transfer delay between amplifier output and the output data is t_{db}. The entire transfer delay from the input data to the output data is around 5 μs, which is very small compared with the traditional wireless data transmission technologies such as Bluetooth, ZigBee, Wi-Fi, and RF communication. However, it should be noted that the long transfer delay of the traditional wireless data transmission methods may be caused by their complicated protocol.

C. Measured Bode Plot of the Data Transfer Capacity

Since the power transfer frequency is difficult to be adjusted while maintaining the primary and secondary resonance, and the gain G_{pd} (from I_i to V_{op}) shown in Figs. 10 and 11 is very small, we only measured the Bode plot of the data transfer capacity (G_{dd}) and the results are shown in Fig. 19, where the data carrier frequency is selected as: 5, 8, 9, 10, 11, 15, 17, and 18 MHz. The red line indicates the Bode plot when *vh* is 2 cm with no lateral drift. The blue line indicates the Bode plot when *vh* is 2 cm and the lateral drift ratio is 30%. The green line indicates the Bode plot when *vh* is 5 cm with no lateral drift.

As can be seen from Fig. 19, G_{dd} reaches its maximum value when the data carrier frequency is around 10 MHz. When the vertical height *vh* or the lateral drift ratio *ldr* becomes larger, the gain G_{dd} gets relatively smaller. The measured trends around 10 MHz match well with the theoretical Bode plots as shown in Figs. 10 and 11.

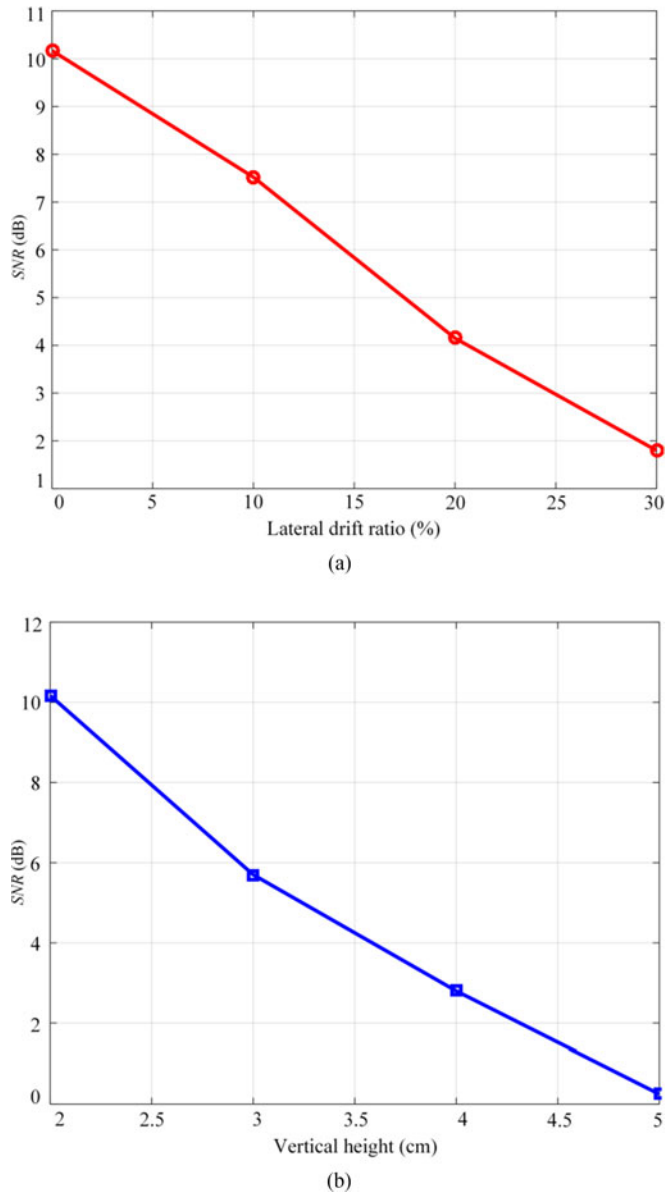

Fig. 16. SNR when the lateral drift ratio and vertical height varies. (a) Lateral drift ratio varies from 0% to 30%; and (b) vertical height varies from 2 to 5 cm.

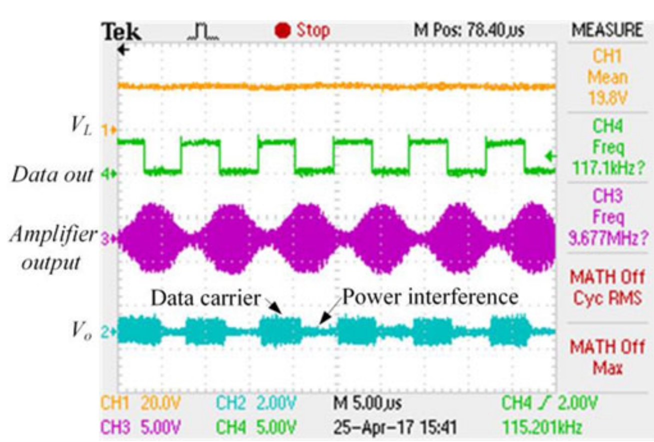

Fig. 17. Parallel power transfer and backward data transfer.

TABLE IV
COMPARISON BETWEEN THE PROPOSED METHOD AND TRADITIONAL METHOD

	Volume of coupling structure	Design of receiving circuit	Spatial position offset redundancy
Inductive way with separated channel [10]	Large	Easy	Small
Inductive way with shared channel [1], [7], [9]	Small	Difficult	Small
Proposed method	Small	Easy	Large

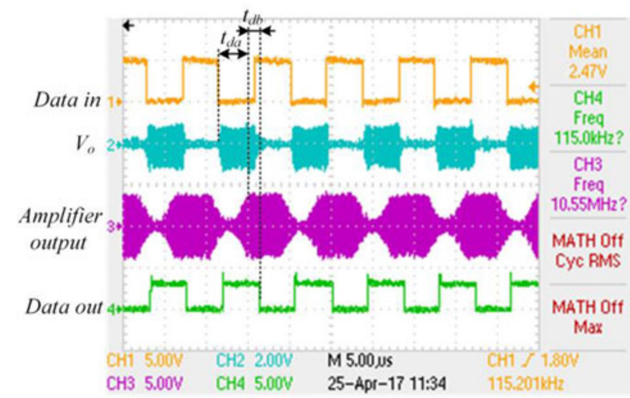

Fig. 18. Time delay of the data transfer.

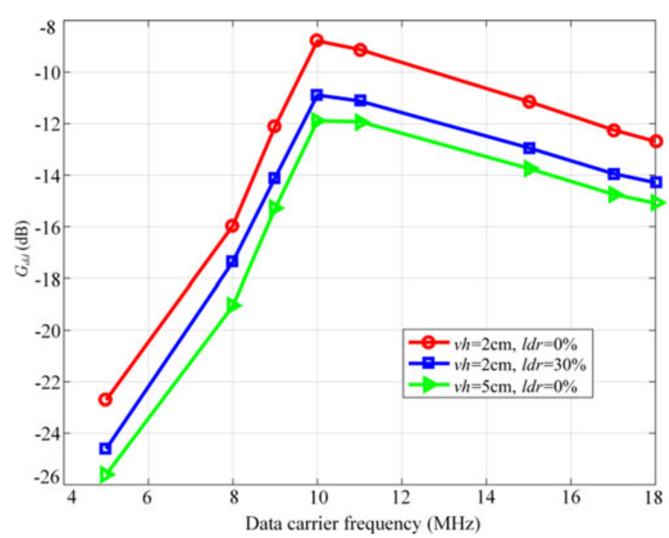

Fig. 19. Measured Bode plot of the data transfer capacity (G_{dd}).

VI. CONCLUSION

A parallel transmission method of power and data is proposed for peer-to-peer WPT systems. With the proposed method, the WPT system achieves power transfer through magnetic field and data transfer through electric field. Coupling structure and operation principle are illustrated and analyzed. Besides, the SNR performance related to the interference of power transfer on data transfer and the data transfer capacity is studied and optimized. Experimental results have shown that the data transfer almost has no effect on power transfer, and the proposed method has the advantage of good flexibility and large spatial position offset redundancy.

ACKNOWLEDGMENT

The authors would like to thank M. Qin, Y. Zhou, and R. Tan for providing the assistance to this paper.

REFERENCES

[1] Y. Sun, P. X. Yan, Z. H. Wang, and Y. Y. Luan, "The parallel transmission of power and data with the shared channel for an inductive power transfer system," *IEEE Trans. Power Electron.*, vol. 31, no. 8, pp. 5495–5502, Aug. 2016.

[2] F. Lu, H. Zhang, H. Health, and C. C. Mi, "An inductive and capacitive combined wireless power transfer system with LC-compensated topology," *IEEE Trans. Power Electron.*, vol. 31, no. 12, pp. 8471–8482, Dec. 2016.

[3] F. Lu, H. Zhang, H. Hofmann, and C. C. Mi, "An inductive and capacitive integrated coupler and its LCL compensation circuit design for wireless power transfer," *IEEE Trans. Ind. Appl.*, 2017, to be published, doi: 10.1109/TIA.2017.2697838.

[4] A. M. Sodagar and P. Amiri, "Capacitive coupling for power and data telemetry to implantable biomedical microsystems," in *Proc. Neural Eng.*, 2009, pp. 411–414.

[5] K. V. T. Piippoen, R. Sepponen, and E. Pekka, "A biosignal instrumentation system using capacitive coupling for power and signal isolation," *IEEE Trans. Biomed. Eng.*, vol. 54, no. 10, pp. 1822–1828, Oct. 2007.

[6] M. Uddin and T. Nadeem, "RF-Beep: A light ranging scheme for smart devices," in *Proc. IEEE Int. Conf. Pervasive Comput. Commun.*, 2013, pp. 114–122.

[7] J. Wu, C. Zhao, Z. Lin, J. Du, Y. Hu, and X. He, "Wireless power and data transfer via a common inductive link using frequency division multiplexing," *IEEE Trans. Ind. Electron.*, vol. 62, no. 12, pp. 7810–7820, Dec. 2015.

[8] C. C. Huang, C. L. Lin, and Y. K. Wu, "Simultaneous wireless power/data transfer for electric vehicle charging," *IEEE Trans. Ind. Electron.*, vol. 64, no. 1, pp. 682–690, Jan. 2017.

[9] Q. Hu, D. Hu, B. Duan, and J. He, "A fully implantable stimulator with wireless power and data transmission for experimental investigation of epidural spinal cord stimulation," *IEEE Trans. Neural Syst. Rehabil. Eng.*, vol. 23, no. 4, pp. 683–692, Jul. 2015.

[10] G. Wang, P. Wang, and Y. Tang, "Analysis of dual band power and data telemetry for biomedical implants," *IEEE Trans. Biomed. Circuits Syst.*, vol. 6, no. 3, pp. 208–215, Jun. 2012.

[11] X. K. Mao and W. Chen, "More precise model for parasitic capacitances in high-frequency transformer," in *Proc. IEEE 33rd Annu. IEEE Power Electron. Spec. Conf.*, 2002, pp. 1054–1057.

[12] S. C. Tang, S. Y. Hui, and H. S. H. Chung, "Characterization of coreless printed circuit board (PCB) transformers," *IEEE Trans. Power Electron.*, vol. 15, no. 6, pp. 1275–1282, Nov. 2000.

[13] S. C. Tang, S. Y. Hui, and H. S. H. Chung, "Coreless planar printed-circuit-board (PCB) transformers—A fundamental concept for signal and energy transfer," *IEEE Trans. Power Electron.*, vol. 15, no. 5, pp. 931–941, Sep. 2000.

[14] M. B. Shadmand and R. S. Balog, "A finite-element analysis approach to determine the parasitic capacitances of high-frequency multiwinding transformers for photovoltaic inverters," in *Proc. Power Energy Conf. Illinois*, 2013, pp. 114–119.

[15] K. Wang and S. Sanders, "Contactless USB—A capacitive power and bidirectional data transfer system," in *Proc. IEEE Appl. Power Electron. Conf. Expo.*, 2014, pp. 1342–1347.

[16] A. Abdolkhani, A. P. Hu, and N. K. C. Nair, "A double stator through-hole type contactless slip ring for rotary wireless power transfer applications," *IEEE Trans. Energy Convers.*, vol. 29, no. 2, pp. 426–434, Jan. 2014.

[17] N. Alireza, M. J. Shokrollahi, and M. Jafar, "A current-fed parallel resonant push-pull inverter with a new cascaded coil flux control for induction heating applications," *J. Power Electron.*, vol. 11, no. 5, pp. 632–638, Sep. 2011.

[18] A. R. Namadmalan, B. Abdi, and J. S. Moghani, "Current-fed parallel resonant push-pull inverter with coil flux control for induction heating applications," in *Proc. Power Electron. Drive Syst. Technol. Conf.*, 2010, pp. 186–190.

[19] D. Wang, K. S. Chin, W. Che, Y. Wu, and C. C. Chang, "Compact 60 GHz low-temperature cofired ceramic filter with quasi-elliptic bandpass response," *IET Microw. Antennas Propag.*, vol. 10, no. 6, pp. 664–669, Apr. 2016.

Xiaofei Li (S'16) received the B.E. degree in Automation from College of Automation, Chongqing University, Chongqing, China, in 2013, where he is currently working toward the Ph.D. degree in the control theory and control engineering.

His research interests include modeling and control of wireless power transfer and power electronics.

Chunsen Tang (S'08–M'09) received his B.E. degree in Automation and his Ph.D. degree in Control Theory and Control Engineering from College of Automation, Chongqing University, Chongqing, China, in 2004 and 2009, respectively.

In 2008, he was a Research Fellow in the Department of Electrical and Computer Engineering, The University of Auckland, Auckland, New Zealand. In 2009, he joined the College of Automation, Chongqing University, where he is currently an Associate Professor. His current research interests include nonlinear modeling and analysis, intelligent control, and wireless power transfer.

Xin Dai (M'10) received the B.E. degree in industrial automation from Yuzhou University, Chongqing, China, in 2000, and the Ph.D. degree in control theory and control engineering from the College of Automation, Chongqing University, Chongqing, China, in 2006.

In 2012, he was a Visiting Scholar with The University of Auckland, Auckland, New Zealand. He is currently a Professor in the College of Automation, Chongqing University. His current research interests include inductive power transfer technology and nonlinear dynamic behavior analysis of power electronics.

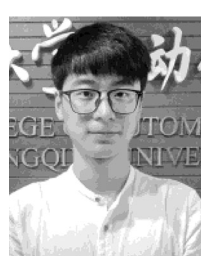

Pengqi Deng received the B.E. degree in Automation from College of Automation, Chongqing University, Chongqing, China, in 2015, where he is currently working toward the Ph.D. degree in the control theory and control engineering.

His research interests include modeling and control optimization of the wireless power transfer.

Yugang Su (M'09) received the B.E. and M.E. degrees in industry automation and the Ph.D. degree in control theory and control engineering from Chongqing University, Chongqing, China, in 1985, 1993, and 2004, respectively.

From 2008 to 2009, he was a Visiting Scholar with the University of Queensland, Brisbane, Australia. He is currently a Professor in the College of Automation, Chongqing University. His research interests include power electronics, control theory and applications, and wireless power transfer.